JOURNAL OF GEOPHYSICAL RESEARCH: PLANETS, VOL. 118, 2558–2569, doi:10.1002/2013JE004499, 2013

# Dissipation at tidal and seismic frequencies in a melt-free, anhydrous Mars

F. Nimmo[1] and U. H. Faul[2]

Received 9 August 2013; revised 1 November 2013; accepted 13 November 2013; published 23 December 2013.

[1] The measured inward motion of Phobos provides a constraint on the tidal dissipation factor, $Q$, within Mars. We model viscoelastic dissipation inside a convective Mars using a modified Burgers model based on laboratory experiments on anhydrous, melt-free olivine. The model tidal $Q$ is highly sensitive to the mantle potential temperature and grain size assumed but relatively insensitive to the bulk density and rigidity structure. $Q$ thus provides a tight constraint on the Martian interior temperature. By fitting the observed tidal $Q$ and tidal Love number ($k_2$) values and requiring present-day melt generation, we estimate that for a grain size of 1 cm the current mantle potential temperature is $1625 \pm 75$ K, similar to that of the Earth. This estimate is consistent with recent petrologically derived determinations of mantle potential temperature but lower than estimates in some thermal evolution models. The presence of water in the Martian mantle would reduce our estimated temperature. Our preferred mantle grain size of $\approx$1 cm is somewhat larger than that of the Earth's upper mantle. The predicted mantle seismic $Q$ is about 130 and is almost independent of depth. The Martian lithosphere represents a high seismic velocity lid, which should be readily detectable with future seismological observations.

**Citation:** Nimmo, F., and U. H. Faul (2013), Dissipation at tidal and seismic frequencies in a melt-free, anhydrous Mars, *J. Geophys. Res. Planets*, *118*, 2558–2569, doi:10.1002/2013JE004499.

## 1. Introduction

[2] The rate at which tidal energy is dissipated within solid bodies can be measured and provides constraints on the interior properties of those bodies. Dissipation is often quantified by a frequency-dependent tidal quality factor $Q$, where large $Q$ means small dissipation. The $Q$ of the solid Earth is 280 at a period of 12.5 h [*Ray et al.*, 2001]; the value of $Q$ for Mars is significantly smaller (see below), indicating more dissipation. On the face of it, this is a surprising result: tides on Mars have shorter periods compared to Earth tides, which should lead to higher, not lower, $Q$ values. Furthermore, simple (Maxwell) viscoelastic dissipation models applied to Mars [*Bills et al.*, 2005] require mantle viscosities that are several orders of magnitude smaller than expected values and are likely inappropriate based on experimental observations. For solid silicate bodies, the tidal $Q$ is highly sensitive to the temperature structure and grain size adopted but relatively insensitive to the density and rigidity structure (see section 5.1 below). $Q$ thus provides a convenient probe of mantle temperature, itself an important indicator of a planet's thermal and volcanic evolution.

[3] In this paper, we apply a dissipation model [*Nimmo et al.*, 2012] based on laboratory experiments [*Jackson and Faul*, 2010] to the case of an anhydrous, melt-free Mars. We show that the measured Martian $Q$ can be generated for reasonable interior structure models. Our preferred model yields a Martian mantle potential temperature similar to that of the Earth's upper mantle. The inferred Martian mantle grain size is larger than that of the Earth's upper mantle, suggesting a higher mantle viscosity for Mars.

### 1.1. Previous Work

[4] Many previous works have modeled the density structure of Mars, using the bulk density and moment of inertia as observational constraints [e.g., *Bertka and Fei*, 1998; *Sohl et al.*, 2005; *Verhoeven et al.*, 2005]. Some have also considered the rigidity (and thus seismic velocity) structure, constrained by the inferred tidal response (Love number) [e.g., *Sohl and Spohn*, 1997; *Van Hoolst et al.*, 2003; *Gudkova and Zharkov*, 2004; *Khan and Connolly*, 2008; *Rivoldini et al.*, 2011]. Unlike many of these works, we do not provide a detailed, multimineral model of Martian density and rigidity, because that is not the aim of this paper. Our primary focus is on the tidal dissipation factor $Q$ which (as we show below) is relatively insensitive to the assumed density and rigidity structures. While we do make use of the Love number and moment of inertia constraints,

[1]Department of Earth and Planetary Sciences, University of California, Santa Cruz, California, USA.
[2]Department of Earth, Atmospheric and Planetary Sciences, Massachusetts Institute of Technology, Cambridge, Massachusetts, USA.

Corresponding author: F. Nimmo, Department of Earth and Planetary Sciences, University of California, 1156 High Street, Santa Cruz, CA 95064, USA. (fnimmo@es.ucsc.edu)


2169-9097/13/10.1002/2013JE004499

we concentrate on $Q$ because it is particularly well suited to determining the mantle temperature structure.

[5] Although the tidal $Q$ of Mars is well known, there have been relatively few attempts to relate it to models of the interior. The most similar approach to ours is briefly described in *Castillo-Rogez and Banerdt* [2013], where the authors adopt an Andrade rheological model and derive a mantle temperature ≈1700 K, assuming dry olivine. *Sohl and Spohn* [1997] adopted a Burgers rheological model but prescribed the ratio (rigidity:unrelaxed rigidity) as a fixed constant rather than calculating it as we do below. *Bills et al*. [2005] showed that a homogeneous, Maxwellian Mars would have to have a viscosity $\approx 10^{15}$ Pa s to match the inferred $Q$, compared with typical terrestrial mantle viscosities of $10^{20}$–$10^{22}$ Pa s. *Efroimsky* [2012] discusses the formalism for applying a hybrid Andrade-Maxwell model to silicate bodies.

[6] *Lognonne and Mosser* [1993] and *Lognonne and Johnson* [2007] briefly discuss the $Q$ of Mars and use an absorption-band model to argue that, other things being equal, a dissipative Mars at tidal frequencies can be reconciled with the known seismic $Q$ of the Earth if the Martian mantle is about 100–150 K colder than that of Earth. As will be seen below, we obtain a similar result if the Martian mantle grain size is comparable to that of the Earth's upper mantle (∼1 mm). However, we favor an alternative in which Earth and Martian mantle temperatures are similar but the Martian mantle has a coarser grain size.

[7] *Zharkov and Gudkova* [1997] outlined how to calculate the tidal $Q$ of a layered Mars and discussed its frequency dependence; they did not, however, use a rheological model to link $Q$ to quantities like temperature or grain size, as we do here. *Khan and Connolly* [2008] included calculations of the $Q$ of Mars, but specific details were not included in the paper.

## 2. Observations

[8] The response of a planetary body to periodic forcing can be described using two parameters: the degree-2 tidal Love number $k_2$, which quantifies the amplitude of the response, and the dissipation factor $Q$, which quantifies the phase lag between forcing and response. The Love number depends on the density and rigidity structure of the body, while $Q$ also depends on whether the body undergoes creep. As a result, $Q$ is much more sensitive to temperature and grain size than is $k_2$. Both $Q$ and $k_2$ are expected to be frequency dependent. In the case of Mars, measurements of both $Q$ and $k_2$ exist at different frequencies and will form our primary observational constraints.

[9] Phobos orbits Mars inside the synchronous point. Dissipation due to tides raised by Phobos on Mars causes Phobos to drift inward at an astrometrically measurable rate [e.g., *Bills et al.*, 2005]. This rate depends on the Martian value of $k_2/Q$ at the synodic period of Phobos (11.106 h). Mars also experiences tides raised by the Sun. Because of Mars' rotation, the solar tides give rise to a periodic term in the gravity field which can be measured [*Yoder et al.*, 2003]. The magnitude of the response depends on the value of $k_2$ at the synodic period of the Sun (24.66 h, roughly Mars' rotation period). Thus, in principle, separate estimates of $k_2$ and $Q$ can be derived. However, there are two complications. First, the measured value of $k_2$ at the solar synodic period will be slightly larger than that at Phobos' period. More seriously, Phobos is sufficiently close to Mars that higher-degree terms ($k_3$, $k_4$, ⋯) affect the rate of orbital evolution [*Bills et al.*, 2005].

[10] *Yoder et al.* [2003] analyzed the response of Mars to solar tides to derive $k_2$. Correcting for the small effects of the fluid core and atmospheric tides, $k_2$ for Mars at 24.66 h period is $0.149 \pm 0.017$. Using our baseline model presented below, $k_2$ is found to be about 0.6% smaller at Phobos' synodic period than at the solar synodic period. Thus, at Phobos' period we estimate $k_2 = 0.148 \pm 0.017$ (0.131–0.165).

[11] *Bills et al.* [2005] included the effects of higher-degree terms in estimating $k_2/Q$ of Mars. However, when inferring $Q$ from $k_2/Q$, they used a value of $k_2 = 0.0745$ appropriate for a homogeneous elastic sphere, which is too low. As a result, their estimate of $Q = 85.58 \pm 0.37$ needs correcting. *Lainey et al.* [2007] used a more realistic value of $k_2 = 0.152$ but explicitly neglected the higher-degree terms. As a result, their estimate of $Q = 79.91 \pm 0.69$ also requires correcting.

[12] To investigate the effect of the higher-degree terms, we will follow *Bills et al.* [2005]. Their equations (13) and (44) can be written

$$\frac{1}{n}\frac{\mathrm{d}n}{\mathrm{d}t} = \frac{k_2}{Q} 9 n \mu \left(\frac{R}{a}\right)^5 \left[1 + 2\frac{k_3}{k_2}\left(\frac{R}{a}\right)^2 + \frac{10}{3}\frac{k_4}{k_2}\left(\frac{R}{a}\right)^4\right] \quad (1)$$

[13] Here $n$ is the mean motion of Phobos, $\frac{1}{n}\frac{\mathrm{d}n}{\mathrm{d}t}$ is its measured secular acceleration, $a$ is the semimajor axis, $R$ is the radius of Mars, and $\mu$ is the Phobos:Mars mass ratio. This expression assumes that the tidal lag angle $\gamma$ is small and frequency independent; the term in square brackets is the correction factor $f$ taking into account higher-degree terms ($k_3$ and $k_4$). If these terms are neglected ($f = 1$), equation (1) shows that the measured secular acceleration can be used to determine $Q$ if $k_2$ is known.

[14] Unfortunately, $k_3$ and $k_4$ are unknown. For a homogeneous body, the correction factor $f = 1.13$ [*Bills et al.*, 2005]. For an inhomogeneous body, this factor (which depends mainly on $k_3/k_2$) will be different. *Van Hoolst et al.* [2003] find Martian model Love numbers $h_2$, $h_3$, and $h_4$ in the range 0.13–0.23, 0.09, and 0.06, respectively. Assuming that the $k$ Love numbers behave similarly, the Van Hoolst et al. results imply that the ratios $k_3/k_2$ and $k_4/k_2$ are in the range 0.39–0.69 and 0.26–0.46, compared with the homogeneous values of 0.435 and 0.252. Taking the upper limits on these ratios, the maximum correction factor $f = 1.20$.

[15] Given estimates of $k_2$ and $f$, equation (1) can then be used to determine $Q$ for Mars. *Lainey et al.* [2007] take $f = 1$ and $k_2 = 0.152$ to derive their value of $Q$; using our preferred values of $f = 1.13 \pm 0.07$ and $k_2 = 0.148 \pm 0.017$, we obtain $Q = 88 \pm 16$. This is very similar to the preferred value of 92 given by *Yoder et al.* [2003]. The values in *Bills et al.* [2005] give $f = 1.13$ and $f\frac{k_2}{Q} = 9.83 \times 10^{-4}$, implying $Q = 170 \pm 20$ for our preferred $k_2$. The source of the discrepancy between these two approaches is unclear but may in part be due to the different time span of observations analyzed in the two studies. For the bulk of this MS we will adopt the *Lainey et al*. [2007] corrected value of $Q = 88 \pm 16$. However, where appropriate we will also discuss the implications of the *Bills et al.* [2005] corrected estimate.

[16] Secondary observational constraints include the moment of inertia ($C/MR^2 = 0.3650 \pm 0.0012$), inferred from the observed precession of the Martian rotation pole [*Yoder et al.*, 2003] and the inferred elastic thickness $T_e$ of the Martian lithosphere. This latter quantity may exceed 300 km at the north pole at present [*Phillips et al.*, 2008] and is estimated at >70 km, 2-80 km, <100 km, and >20 km for four Amazonian-aged features [*McGovern et al.*, 2004]. A compilation by *Grott et al.* [2013] concludes that present-day $T_e$ values exceed 150 km. There is probably spatial variability in $T_e$ as a result of variations in lid thickness induced by convection [*Kiefer and Li*, 2009; *Grott and Breuer*, 2010]. Note that only part of the stagnant, nonconvecting lid will respond in an elastic manner over geological timescales; thus, the stagnant lid thickness is generally greater than the effective elastic thickness.

## 3. Model

[17] In this work we are most interested in dissipation within Mars and the factors which control it (primarily temperature and grain size). We will therefore adopt a relatively elaborate model of the dissipation process (see section 3.2 below). Conversely, our model will in other ways be significantly simplified, e.g., in its treatment of phase changes and its calculation of pressure and density (section 3.1). These simplifications are adopted for three reasons: first, our current knowledge of Mars' internal structure and composition is highly uncertain; second, the approximations involved can be shown a posteriori not to affect our main conclusions; and third, a simplified approach makes the sensitivity of our results to uncertainties more transparent.

[18] Even the dissipation model has its simplifications. In particular, it assumes that the dissipative behavior (but not the density/rigidity structure) of the Martian mantle can be adequately represented by the experimentally characterized response of dry, melt-free $Fo_{90}$ olivine [*Jackson and Faul*, 2010]. In detail, this assumption is unlikely to be correct. The bulk of the Martian mantle is most likely olivine but of a more iron-rich kind than typical terrestrial values [*Dreibus and Wanke*, 1985]. The water content and extent of melting within the Martian mantle are not well known, but both can have significant effects on dissipation. The lower Martian mantle hosts higher-pressure phases (wadsleyite, ringwoodite, and possibly perovskite) [*Longhi et al.*, 1992] which are treated in a simplified manner below.

[19] At one level, our decision to model the dissipative component of the Martian mantle using results from $Fo_{90}$ is a purely pragmatic decision: other minerals and compositions have not been sufficiently well characterized to allow their rheological behavior to be described. However, it also represents a reasonable initial approach: dissipation is likely to be dominated by the most abundant mineral present, and a dry, melt-free mantle represents a useful end-member. We discuss the potential effects of melt and water further below (section 5.1). The simplified treatment of phase changes can be justified a posteriori as our best fit models result in most dissipation happening in the upper (low-pressure) part of the mantle (see Figure 1). The role of iron in controlling olivine dissipation is currently poorly understood but may be quite dramatic [*Zhao et al.*, 2009]; thus, the approach adopted here probably underestimates the dissipation for a given set of conditions.

### 3.1. Bulk Structure

[20] For our simplified Martian structure, we will assume a five-layer model consisting of core, a mantle split into olivine (*ol*), wadsleyite (*wa*), and ringwoodite (*ri*) phase assemblages, and a crust. For the purposes of calculating the gravity and pressure within Mars, we will assume that the mantle and core have constant densities $\rho_m$ and $\rho_c$, respectively. For a specified value of $\rho_c$ we calculate the core radius and mantle density which satisfy the measured bulk density and moment of inertia of Mars, taking the crust into account (see Table 3). This approach is evidently not self-consistent, but the errors introduced are much smaller than other uncertainties (see below).

[21] Taking the core radius to be $R_c$, the gravitational acceleration within the mantle is given by

$$g(r) = \frac{4}{3}\pi G_g \left[ (\rho_c - \rho_m)\frac{R_c^3}{r^2} + r\rho_m \right] \quad (2)$$

where $G_g$ is the gravitational constant, and here we are neglecting the small density contrast between crust and mantle. In the mantle the pressure increment $dP$ is given by $dP = -\rho_m g\, dr$ which yields

$$P(r) = \frac{4}{3}\pi G_g \rho_m \left[ R_c^3 \Delta\rho \left( \frac{1}{r} - \frac{1}{R} \right) + \frac{\rho_m}{2}\left( R^2 - r^2 \right) \right] \quad (3)$$

where $R$ is the radius of Mars and $\Delta\rho = \rho_c - \rho_m$.

[22] In reality, the mantle density $\rho$ will vary with depth because of compressibility, thermal expansion, and phase changes. For a particular phase assemblage $x$, we calculate $\rho_x$ as follows:

$$\rho_x(r) = \rho_{0,x}\left( 1 + \frac{P(r)}{K_x(r)} \right)(1 - \alpha_x[T(r) - T_R]) \quad (4)$$

where $K_x$ is the bulk modulus, $T$ is the temperature, $T_R$ is a reference temperature, and $\alpha_x$ is the thermal expansivity (assumed constant). The quantity $\rho_{0,x}$ is a reference density. In what follows, we vary the reference density $\rho_0$ of the olivine phase so that the bulk density of the mantle equals $\rho_m$. The other two reference densities are kept fixed. The bulk modulus is calculated as described in section 3.2.

[23] While this approach is not fully self-consistent, the errors introduced are small. The difference between the analytical values for $g(r)$ (equation (2)) and those obtained by numerically integrating the calculated density profile (equation (4)) never exceeds 3%. Similarly, the difference between the analytical value for $P(r)$ (equation (3)) and that obtained by numerical integration never exceeds 4%. Given other major uncertainties (notably the location of the core-mantle boundary), such errors are acceptable.

[24] The temperature structure of the Martian mantle likely includes a conductive stagnant lid overlying a convecting adiabatic mantle [e.g., *Ogawa and Yanagisawa*, 2011]. A simple parameterization approximating this behavior may be obtained as follows. The horizontally averaged potential temperature $T_p$ is given by

$$T_p(z) = T_s + (T_m - T_s)\tanh(z/L) \quad (5)$$

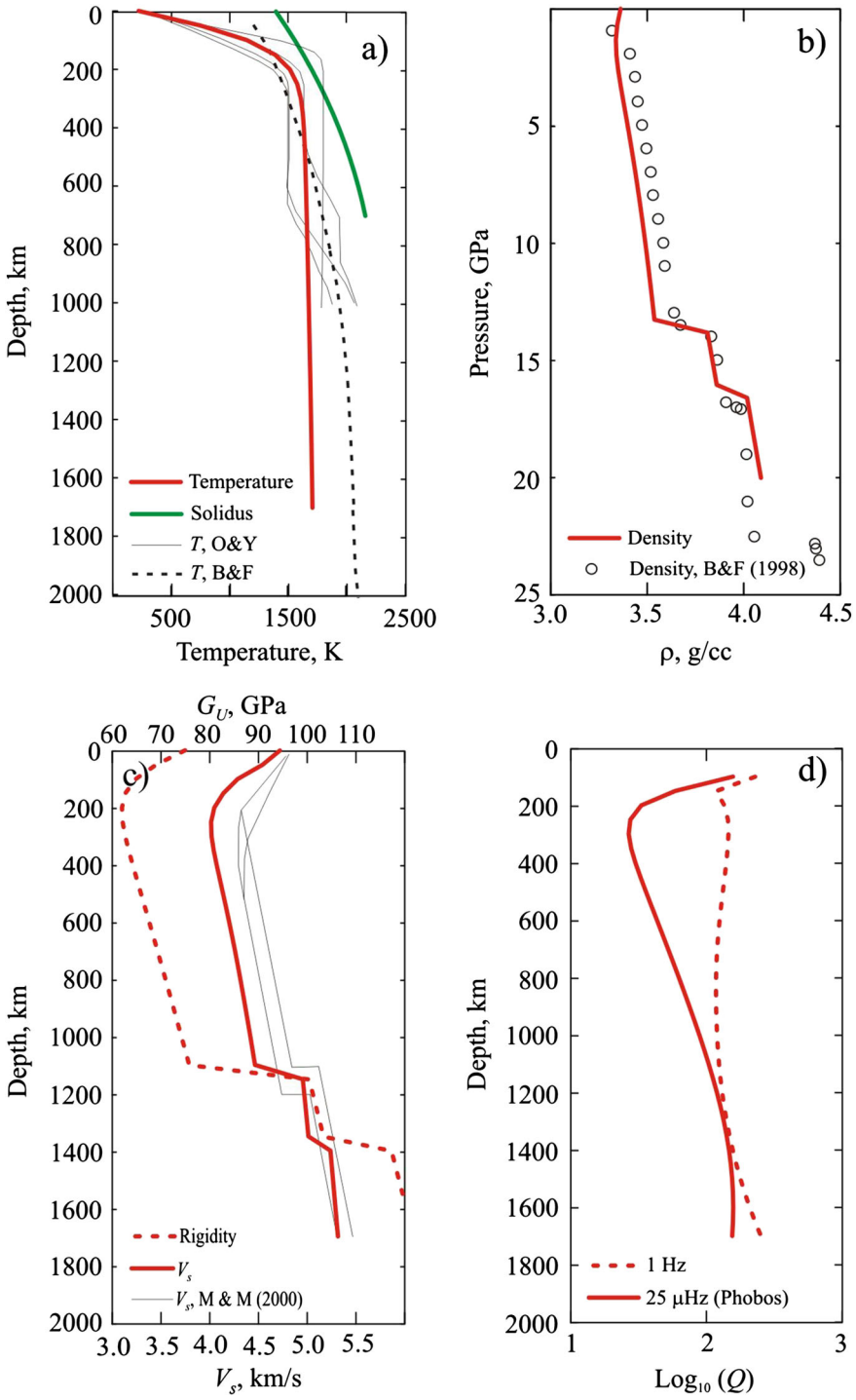


**Figure 1.** (a) Temperature as a function of depth. Bold red line is our preferred model with $L$ = 125 km and $T_m$ = 1600 K (equation (5)). Thin black lines are present-day temperature profiles from different convection runs of *Ogawa and Yanagisawa* [2011]; note that their computational domain is only 1000 km deep. Thick green line is the peridotite solidus of *Hirschmann* [2000]. Dotted line is the petrological geotherm from *Bertka and Fei* [1997]. (b) Density as a function of pressure. Bold red line is our preferred model (equation (4)). Circles are replotted from *Khan and Connolly* [2008, Figure 2] and show calculated mantle densities based on experiments [*Bertka and Fei*, 1998]. (c) Model unrelaxed rigidity modulus $G_U$ (equation (9)) and *S* wave velocity ($V_s = \sqrt{G/\rho}$) at 1 Hz as a function of depth. Thin black lines are two velocity models from *Mocquet and Menvielle* [2000]. (d) Model $Q$ as a function of depth, evaluated at 25μHz (Phobos' synodic period) and at 1 Hz.

[25] Here $T_s$ is the surface temperature, $T_m$ is the potential temperature of the convecting interior, and depth $z = R - r$. The near-surface heat flux in this model is $k(T_m - T_s)/L$, where $k$ is the thermal conductivity. The quantity $L$ is an indication of how thick the conductive lid is; roughly 90% of the total temperature drop occurs across a thickness 1.5 $L$, so we may take the stagnant lid thickness to be $\approx$ 1.5 $L$. Because most materials do not undergo significant creep below about 70% of their melting point [*Frost and Ashby*, 1982], the effective elastic thickness of the lithosphere is approximated by $L$.

[26] To convert from potential temperature to actual temperature $T(z)$, we multiply $T_p(z)$ by an adiabatic factor $f_{ad}$. The adiabatic temperature gradient $dT/dz = \alpha g T/C_p$, where $\alpha$ and $C_p$ are thermal expansivity and specific heat capacity, respectively. Taking these two quantities to be constant and using equation (2) for $g$, we find

$$\ln f_{ad} = \frac{4}{3}\frac{G_g \alpha}{C_p}\left[-\frac{R_c^3}{R}\Delta\rho\frac{z/R}{1-(z/R)} + \rho_m\left(Rz - \frac{z^2}{2}\right)\right] \quad (6)$$

[27] Equations (5) and (6) can thus be combined to derive the real temperature profile.

[28] Our simplified model does not treat the crust in detail. This is because $Q$, our main focus, will not be significantly affected by a cold, thin surficial layer. However, because the crust may be enhanced in radiogenic elements, it will affect the temperature structure; in particular, the conductive heat flux through the lid derived from equation (5) may be less than the actual surface heat flux.

### 3.2. Dissipation Model

[29] Local dissipation in the Martian mantle is calculated by using a model based on laboratory experiments to determine the complex rigidity as a function of depth. We generally adopt the same approach and parameters as in *Nimmo et al.* [2012]; only a summary is given below.

[30] Laboratory experiments on melt-free, polycrystalline olivine show that the dissipation factor $Q$ goes as $\omega^\alpha$, where $\omega$ is the forcing angular frequency and $\alpha$ is a constant $\approx$ 0.3 [e.g., *Gribb and Cooper*, 1998; *Jackson et al.*, 2004]. One advantage of investigating Mars rather than the Moon is that the tidal frequencies are higher ($\sim 10^{-4}$ s$^{-1}$ rather than $\sim 10^{-6}$ s$^{-1}$). This means that, unlike the Moon, essentially no extrapolation in frequency is required when applying the laboratory-derived parameters to Mars.

[31] Qualitatively, dissipation appears to arise from two different mechanisms: a background effect, inferred to be due to a diffusive process and modeled as a distribution of relaxation times, and a superimposed peak corresponding to elastically accommodated grain boundary sliding. Both these mechanisms are included. The result is that $Q$ and the rigidity modulus $G$ are dependent on temperature, pressure, and forcing period. The sensitivity of $Q$ to temperature and frequency is much larger than that of $G$; for Mars-sized objects the pressure sensitivity is minor but not negligible. The results are also sensitive to the grain size $d$ adopted; we examine the effects of varying this parameter below.

[32] In detail, we treat the shear modulus as a complex quantity $G^* = 1/J^*$, where $J^* = J_r + iJ_i$ is the complex compliance and $i = \sqrt{-1}$. At a particular frequency the dissipation factor $Q = J_r/J_i$. For the extended Burgers model, the real and imaginary components of the complex compliance are as follows:

$$J_r(\omega) = \frac{1}{G_U}\left[1 + \Delta\int_{\tau_L}^{\tau_H}\frac{D(\tau)\,d\tau}{(1+\omega^2\tau^2)}\right] \quad (7)$$

and

$$J_i(\omega) = \frac{1}{G_U}\left[\omega\Delta\int_{\tau_L}^{\tau_H}\frac{\tau D(\tau)\,d\tau}{(1+\omega^2\tau^2)} + \frac{1}{\omega\tau_M}\right] \quad (8)$$

[33] Here $G_U = 1/J_U$ is the unrelaxed (infinite-frequency) shear modulus calculated using equation (9) below, $\tau$ is a dummy variable, $\tau_M = \eta/G_U$ is the Maxwell time for a material of steady state viscosity $\eta$, $\Delta$ describes the strength of the relevant relaxation mechanism, $\omega$ is the angular frequency, and $\tau_L$ and $\tau_H$ are the integration limits corresponding to short and long periods, respectively. In the low-frequency limit, equation (8) reduces to Maxwellian behavior, in which $J_i = (\omega\eta)^{-1}$.

[34] As noted above, laboratory experiments suggest that there are two different relaxation mechanisms operating, with different distributions of relaxation times. We therefore include both a high-temperature background with strength $\Delta_B$ and an additional peak with strength $\Delta_P$. Both distributions are a strong function of grain size and temperature. Further details may be found in *Jackson and Faul* [2010] and *Nimmo et al.* [2012]. Unless noted otherwise below, all rheological parameters used are identical to those given in *Nimmo et al.* [2012, Table 1]; one exception is the reference grain size (13.4 $\mu$m) which was incorrectly stated to be 3.1 $\mu$m in that paper.

[35] The elastic (unrelaxed) rigidity modulus $G_U$ depends on pressure and temperature and is calculated as in *Nimmo et al.* [2012]:

$$G_U(T,P) = G_U(T_R,P_R) + (T-T_R)\frac{\partial G}{\partial T} + (P-P_R)\frac{\partial G}{\partial P} \quad (9)$$

where $P_R$ and $T_R$ are the reference temperature and pressure, and $\frac{\partial G}{\partial T}$ and $\frac{\partial G}{\partial P}$ are experimentally measured quantities (see below). Note that here we have neglected higher-order pressure derivatives, owing to the relatively modest pressures on Mars. We adopt different values of the reference rigidity $G_U(T_R, P_R)$ and the partial derivatives for the three different phases (see Table 1).

[36] We calculate the (unrelaxed) bulk modulus $K$ in an analogous fashion:

$$K(T,P) = K(T_R,P_R) + (T-T_R)\frac{\partial K}{\partial T} + (P-P_R)\frac{\partial K}{\partial P} \quad (10)$$

The bulk modulus is assumed to not vary significantly with period, but is important in determining the density structure (equation (4)).

[37] The calculations detailed in *Nimmo et al.* [2012] yield the complex shear modulus $G$ at a specified frequency, where the ratio of the real to the imaginary parts of the modulus contains information on the local value of $Q$. At high frequencies, the mantle response is essentially elastic and $G \approx G_U$. At lower frequencies, dissipation becomes more important and $G < G_U$. To calculate the global, frequency-dependent quantities $Q$ and $k_2$, the method of *Roberts and Nimmo* [2008] is used. The mantle is discretized into layers 50 km thick, while the core is assumed to be fully

**Table 1.** Parameter Values for the Nominal Model[a]

| Quantity | Value | Units | Eqn. | Quantity | Value | Units | Eqn. |
|---|---|---|---|---|---|---|---|
| $R$ | 3400 | km | 3 | $R_c$ | 1700 | km | 2 |
| $\rho_m$ | 3526 | kg m$^{-3}$ | 2 | $\rho_c$ | 7000 | kg m$^{-3}$ | 2 |
| $T_s$ | 220 | K | 5 | Olivine assemblage (*ol*) | | | |
| $L$ | 125 | km | 5 | $\rho_0$ | 3300 | kg m$^{-3}$ | 4 |
| $T_R$ | 1173 | K | 9 | $G_U(T_R, P_R)$ | 62.7 | GPa | 9 |
| $P_R$ | 0.2 | GPa | 9 | $\partial G/\partial T$ | -13.1 | MPa K$^{-1}$ | 9 |
| $d$ | 1 | cm | - | $\partial G/\partial P$ | 1.5 | - | 9 |
| $T_m$ | 1600 | K | 5 | $\alpha$ | $2 \times 10^{-5}$ | K$^{-1}$ | 6 |
| $C_p$ | 1200 | J kg$^{-1}$ K$^{-1}$ | 6 | $K(T_R, P_R)$ | 114 | GPa | 10 |
| | | | | $\partial K/\partial T$ | -18 | MPa K$^{-1}$ | 10 |
| | | | | $\partial K/\partial P$ | 4.2 | - | 10 |
| Wadsleyite assemblage (*wa*) | | | | Ringwoodite assemblage (*ri*) | | | |
| $\rho_0$ | 3580 | kg m$^{-3}$ | 4 | $\rho_0$ | 3770 | kg m$^{-3}$ | 4 |
| $G_U(T_R, P_R)$ | 88.8 | GPa | 9 | $G_U(T_R, P_R)$ | 102 | GPa | 9 |
| $\partial G/\partial T$ | -15 | MPa K$^{-1}$ | 9 | $\partial G/\partial T$ | -15 | MPa K$^{-1}$ | 9 |
| $\partial G/\partial P$ | 1.4 | - | 9 | $\partial G/\partial P$ | 1.4 | - | 9 |
| $\alpha$ | $2 \times 10^{-5}$ | K$^{-1}$ | 6 | $\alpha$ | $2 \times 10^{-5}$ | K$^{-1}$ | 6 |
| $K(T_R, P_R)$ | 159 | GPa | 10 | $K(T_R, P_R)$ | 167 | GPa | 10 |
| $\partial K/\partial T$ | -12 | MPa K$^{-1}$ | 10 | $\partial K/\partial T$ | -29 | MPa K$^{-1}$ | 10 |
| $\partial K/\partial P$ | 4.3 | - | 10 | $\partial K/\partial P$ | 4.1 | - | 10 |

[a]Other rheological parameters are identical to those given in *Nimmo et al.* [2012, Table 1] except the reference grain size (13.4 μm). "Eqn." stands for equation.

liquid (zero shear modulus) and have other properties given in Table 1. The outermost 50 km thick layer is taken to be the crust, with an assumed density of 2900 kg m$^{-3}$ and the same elastic parameters as mantle material. We assume that Mars is spherically symmetric.

[38] The Martian mantle, like that of the Earth, is expected to undergo phase changes [*Longhi et al.*, 1992; *Bertka and Fei*, 1997]. The olivine-wadsleyite and wadsleyite-ringwoodite transitions are expected to occur at roughly 1100 km and 1400 km depths, respectively [e.g., *Mocquet and Menvielle*, 2000; *Khan and Connolly*, 2008], depending on composition and temperature. The depth to the perovskite transition is comparable to the mantle thickness, so whether or not it occurs depends on details of the model adopted, such as the core radius and mantle temperature [*Bertka and Fei*, 1997]. For simplicity, we fix the transition depths $z_{ol\text{–}wa}$ =1150 km and $z_{wa\text{–}ri}$ = 1400 km and neglect the perovskite phase entirely. The anelastic behavior of these higher-pressure phases has not yet been fully characterized [*Nishihara et al.*, 2008; *Kawazoe et al.*, 2010]. However, seismological observations on Earth suggest that $Q$ does not increase in a discontinuous fashion at the top of the transition zone. Rather, most models show a continuous increase through the upper mantle and the transition zone [*Matas and Bukowinski*, 2007]. Thus, to first order it appears that the dissipative nature of the mantle material is not changed by the *ol-wa* or *wa-ri* phase transitions. To calculate the anelastic behavior of the higher-pressure assemblages, we therefore adopt the same parameters describing dissipation as for the olivine assemblage. Note, however, that $\rho_0$ and $G_U$ and $K$ and their derivatives are different (see Table 1).

### 3.3. Parameters Adopted

[39] Except as noted below, the material properties of the mantle are taken from *Jackson and Faul* [2010, Table 2]. These authors were using $Fo_{90}$ olivine; more iron-rich olivine (likely appropriate for Mars) will have slightly different elastic properties [*Bass*, 1995]. For all three phases we obtain $G_U(T_R, P_R)$ and $K(T_R, P_R)$ and their derivatives from *Stixrude and Lithgow-Bertelloni* [2005, 2011] for an Mg# of 75; equations (9) and (10) are then used to determine $G_U$ and $K$ at the conditions of interest. With this approach we are assuming that the higher iron content only affects the elastic moduli but not the grain boundary viscosity or diffusivity of olivine. The latter assumption can be justified by the observation that silicon is the slowest-diffusing species, controlling strain rates for both grain boundary and volume diffusion [e.g., *Hirth and Kohlstedt*, 2003; *Dohmen and Milke*, 2010]. On a more pragmatic level, there are currently no experimental data on dissipative behavior in iron-rich olivines.

[40] The three reference densities $\rho_0$ were chosen to approximately satisfy the petrologically derived density curve of *Bertka and Fei* [1998] (see Figure 1b) while yielding the observed moment of inertia and bulk density. Varying these values has no significant effect on the resulting $Q$ (see section 5.1). The thermal expansivities were likewise chosen to approximately match the more sophisticated calculations of *Sohl and Spohn* [1997, Figure 4]; likely variations have only minor effect on our results (section 5.1).

[41] Our baseline core parameters were chosen to be consistent with the observed bulk density and moment of inertia. We examine the effect of varying these parameters below (section 5.1) and conclude that, although they do affect the model $k_2$, they have almost no effect on the model $Q$ value. We emphasize again that $Q$ is sensitive to temperature and grain size but not rigidity or density. As a result, more sophisticated and self-consistent models of rigidity and density will not produce appreciably different dissipation results compared with the simple models we have adopted here.

## 4. Results

[42] Figure 1 plots the result of our nominal model, for which $L$ = 125 km, $T_m$ = 1600 K, and $d$ = 1 cm. Figure 1a

**Table 2.** Model Results and Comparison With Observations[a]

| | $T_m$ (K) | $L$ (km) | $d$ (mm) | $Q$ (Phobos) | $k_2$ (Phobos) | $k_2$ (1 Hz) | $\Delta T_{sol}$ (K) |
|---|---|---|---|---|---|---|---|
| Models | 1600 | 125 | 10 | 89 | 0.141 | 0.136 | 199 |
| | 1600 | 150 | 10 | 92 | 0.141 | 0.136 | 247 |
| | 1590 | 100 | 10 | 89 | 0.141 | 0.136 | 149 |
| | 1610 | 200 | 10 | 96 | 0.140 | 0.136 | 332 |
| | 1450 | 150 | 1 | 98 | 0.138 | 0.132 | 389 |
| Observed | - | - | - | $88 \pm 16$ | $0.148 \pm 0.017$ | - | |

[a]Because $Q$ and $k_2$ are frequency dependent, we specify the period at which they are evaluated. $\Delta T_{sol}$ gives the smallest difference between the mantle temperature and the solidus temperature and quantifies how easy it is to generate melt. The final row gives the observational constraints, as described in section 2.

compares our model mantle temperature (red line) with the present-day mean values obtained from a suite of convection models (black lines) [*Ogawa and Yanagisawa*, 2011]. Given the simplifications in our model, the agreement is quite good. The main difference is that our temperature model does not include the effects of compositional layering, which give rise to non-adiabatic behavior toward the base of the mantle.

[43] We also plot the dry peridotite solidus of *Hirschmann* [2000] (thick green line). This curve shows where melting is most likely to occur. Since Mars is iron-rich, the actual solidus may differ slightly from that shown here [e.g., *Bertka and Holloway*, 1994]. If the interior of Mars is wet, the solidus temperatures will be significantly reduced, making the production of minor amounts of melt more likely (see below). Finally, we also plot the "areotherm" used by *Bertka and Fei* [1997] (dotted line). This line was used in a set of petrological experiments on Mars analog materials; it was not intended to represent an actual likely areotherm and is evidently too warm in the top few hundred kilometers.

[44] Figure 1b plots the nominal model density structure as a function of pressure. Density in the lid does not vary much, because the thermal expansivity effect approximately cancels the competing effect of self-compression. In the convecting mantle, the temperature variations are small and thus density increases with depth. We compare our results with the measurements of *Bertka and Fei* [1998] on analog Mars mantle material. In the upper mantle our model densities are slightly lower than the *Bertka and Fei* [1998] measurements. This is a consequence of having to match the bulk density and moment of inertia constraints given our assumed core radius and density. Increasing $\rho_0$ to match the measurements has no effect on the resulting model $Q$. In the lower mantle ($z$ >1150 km) our density profile agrees reasonably well with the measured values.

[45] Figure 1c plots our model unrelaxed shear modulus and shear wave velocity $V_s = \sqrt{G/\rho}$ (evaluated at 1 Hz). We compare our $V_s$ profile with two model results from *Mocquet and Menvielle* [2000]; the agreement is close, except that our velocities are slightly lower than theirs in the shallow mantle, because we are using slightly different elastic parameters.

[46] A particularly important result of both *Mocquet and Menvielle* [2000] and *Rivoldini et al.* [2011]—which our study replicates—is the high-velocity lid. This arises because the lid has relatively high-temperature gradients, and thus the effect of temperature on $G$ is more important than the effect of pressure. The changes in pressure and temperature across the lid are roughly 2.5 GPa and 1400 K, resulting in changes in $G_U$ of +4.5 GPa and –19 GPa, respectively. Since the density changes only slightly, the result is a reduction in shear velocity with increasing depth within the lid. This effect is more pronounced than on Earth because temperature gradients are similar on the two planets but the pressure gradient is a factor of 3 lower on Mars.

[47] Some previous works did not find a high-velocity lid [e.g., *Gudkova and Zharkov*, 2004; *Khan and Connolly*, 2008]. This is because they used the *Bertka and Fei* [1997] areotherm (Figure 1a), which has a temperature drop across the top 250 km of about 300 K. The resulting changes in $G_U$ from pressure and temperature effects in this case are +5.8 GPa and –3.4 GPa; as a result, rigidity increases continuously with depth and no high-velocity lid is predicted.

[48] Finally, Figure 1d plots $Q$ as a function of depth at both seismic (1 Hz) and tidal frequencies. The most important result is that $Q$ is minimized and tidal dissipation is maximized just below the lid. This occurs because the mantle is almost isothermal, so the main control on $Q$ as a function of depth is the activation volume [*Nimmo et al.*, 2012, equation (6)]. This result is in contrast to the findings of *Zharkov and Gudkova* [1997], who did not consider the effects of pressure on $Q$. Because the main locus of tidal dissipation is in the upper mantle, our simplified treatment of the phase transitions at depth is unlikely to significantly affect our results. At seismic periods, $Q$ is approximately constant (≈130) but increases steeply within the lid, because of the cold temperatures there. The actual $Q$ in this region is likely to be smaller, because of scattering in the shallow crust (as on the Moon—an effect not modeled here).

[49] For our preferred model shown in Figure 1, the bulk $Q$ at Phobos frequencies is 89, in the middle of the estimated range of 72–104. The model $k_2$ at Phobos frequencies is 0.141, in the middle of the inferred range of 0.131–0.165. Table 2 summarizes the results from this model and several comparable ones. As will be seen below, $Q$ provides a far more stringent constraint on the temperature structure of Mars than does $k_2$; $k_2$ is more sensitive to the density structure (e.g., core radius).

### 4.1. Trade-Off Between Lid Thickness L and Mantle Temperature $T_m$

[50] Figure 2 plots how $k_2$ and $Q$ vary with the lid thickness $L$ and mantle potential temperature $T_m$ for a grain size of 1 cm. Figure 2a shows that increasing $T_m$ increases

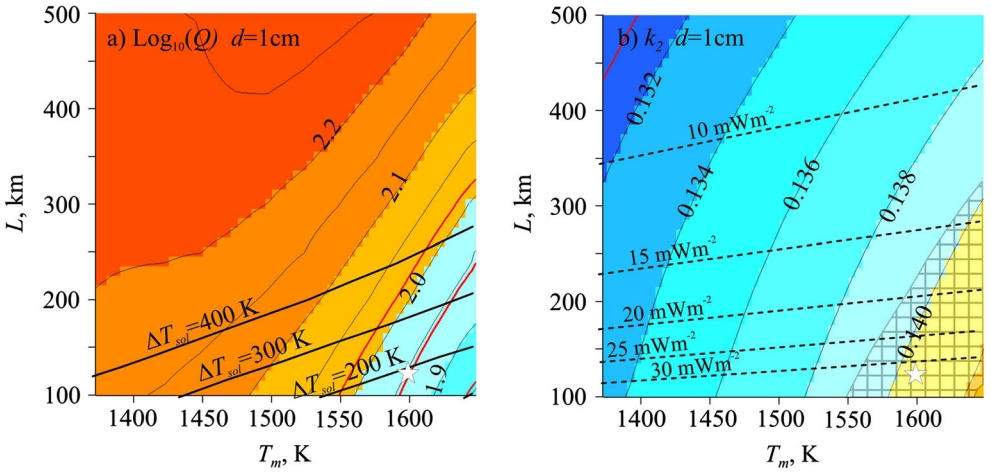


**Figure 2.** (a) Log10 of Martian $Q$ evaluated at Phobos' synodic period, as a function of lid thickness $L$ and mantle potential temperature $T_m$ with grain size $d$ = 1 cm. Red lines denote upper, lower, and mean inferred Martian $Q$ values (Table 2). Solid black lines are contours of $\Delta T_{sol}$ (see text). Melting is less likely as $\Delta T_{sol}$ increases. Star denotes preferred model (Figure 1). (b) As in Figure 2a but showing contours of Martian $k_2$ evaluated at the same period. Red line is the lower bound on the observed $k_2$. Hatched region shows the parameter space satisfying $Q$. Dashed lines contour conductive heat flux through the lid, taking the thermal conductivity to be 3 W m$^{-1}$ K$^{-1}$.

dissipation (decreases $Q$), as expected, while a thicker lid reduces dissipation. Similarly, in Figure 2b a thicker lid reduces $k_2$ (because an elastic lid reduces the amplitude of tidal deformation), while increasing $T_m$ increases $k_2$ (because a warmer planet is more deformable).

[51] The red lines in Figure 2a show the estimated range of $Q$ for Mars, and the white star denotes our nominal model (Figure 1). There is evidently a trade-off between $L$ and $T_m$: a thicker lid requires a hotter mantle to match the observed value (see Table 2). However, the sensitivity to lid thickness is not very great: for a constant $Q$, increasing $L$ by 100 km requires an increase in $T_m$ by only 40 K.

[52] The red line in Figure 2b shows the lower bound on $k_2$. Compared to $Q$, $k_2$ varies rather little with temperature and thus does not provide a strong constraint on $T_m$. The cross-hatched region in Figure 2b shows the parameter space in which $Q$ is satisfied. For $L$ >100 km, the mantle potential temperature $T_m$ has to exceed 1550 K. To further constrain $L$ and $T_m$ requires other arguments, presented in the following section.

[53] Figure 3 is identical to Figure 2 but shows what happens for a smaller grain size ($d$ = 1 mm). Smaller grains result in lower $Q$ and lower rigidities; as a result, matching the observations requires correspondingly lower mantle temperatures. As before, the cross-hatched region in Figure 3b shows the parameter space in which $Q$ is satisfied, while $k_2$ does not provide a tight constraint. Depending on the value of $L$ adopted, temperatures could be anywhere in the range 1420–1650 K. We will argue below that values of $L$ in the range 100–200 km are more likely, in which case temperatures cannot exceed 1525 K. This result is reminiscent of the suggestion made by *Lognonne and Mosser* [1993] that the bulk $Q$ of Mars can be explained if its mantle is colder than that of the Earth.

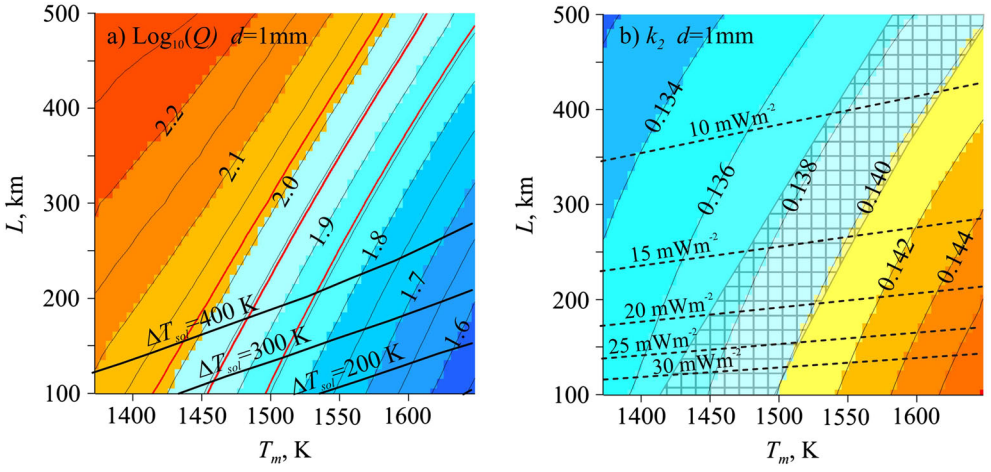


**Figure 3.** As in Figure 2 but assuming the grain size $d$ = 1 mm. Note that the acceptable parameter space has shifted to lower temperatures.

### 4.2. Degeneracies

[54] Figures 2 and 3 demonstrate that different combinations of $T_m$, $L$, and $d$ can satisfy the observational constraints. Here we discuss how these degeneracies can be reduced.

[55] The main additional constraint is to consider the importance of melting. *Hartmann et al.* [1999] used crater counts to deduce volcanism happening within the last 1–2% of Mars' history, presumably as a result of plume activity (see also *Vaucher et al.* [2009]). For such volcanism to occur, the mantle temperature must exceed the solidus, at least locally. As shown in Figure 1, this is most likely to occur close to the base of the lid. Figures 2a and 3a contour the smallest temperature difference between the mean mantle temperature and the solidus temperature, $\Delta T_{sol}$. For instance, for our nominal model the smallest difference is $\Delta T_{sol}$ = 199 K. Evidently, smaller lid thicknesses make it easier to simultaneously satisfy the requirements of $Q$, $k_2$, and melt generation. Furthermore, comparison of Figures 2a and 3a show that it is harder to satisfy all three requirements with a small grain size, because the lower mantle temperatures make it difficult to generate melt.

[56] In a convecting mantle, upwellings will be hotter than the average mantle temperature and the local stagnant lid thickness will be reduced [e.g., *Solomatov and Moresi*, 1996]. Full calculations of convective melt production are beyond the scope of this work, but we can provide some rough constraints as follows. *Kiefer* [2003] states that a lid thickness of about 270 km ($L \approx$180 km in our terms) produces no melt in a model with a potential temperature of 1804 K. Although much hotter than our models, this result suggests that $\Delta T_{sol} \approx 150 - 200$ K is enough to stop melting. With a mantle potential temperature $T_m$ = 1600 K, $\Delta T_{sol}$ = 199 K for $L$ = 125 km and 140 K for $L$ = 100 km (Figures 2,3), suggesting that localized melt production should be possible in these cases. Furthermore, inspection of Figure 1a shows the close similarity between our nominal temperature profile ($L$ = 125 km) and the profile from model CM7H of *Ogawa and Yanagisawa* [2011], for which melting occurs at the present day.

[57] Evidently, melting depends sensitively on the value of $L$ adopted. *McGovern et al.* [2004] estimated heat flux upper bounds of 24 and 28 mW m$^{-2}$ for two Amazonian-age volcanic features. Figure 2b shows that such values imply $L \geq$150 km, in rough agreement with the bounds discussed above. Conversely, the *Phillips et al.* [2008] value of $L$ = 300 km estimated at the north pole of Mars would result in no melting at all and is presumably reflective of local rather than global conditions [*Kiefer and Li*, 2009; *Grott and Breuer*, 2010].

[58] Overall, values of $L$ in the range 100–200 km seem most likely. Under this assumption, the $d$ = 1 cm cases (Figure 2) can simultaneously satisfy the requirements of $k_2$, $Q$, and melt production. For $L$ in the range 100–200 km, the range of $T_m$ within which $Q$ is satisfied is roughly 1550–1700 K. Conversely, for $d$ = 1 mm the temperatures required to satisfy the tidal ($Q$, $k_2$) constraints are so low that simultaneously generating melt is very problematic.

[59] In summary, the tidal constraints ($k_2$ and $Q$) permit some pairs of $T_m$ and $L$ values. The requirement for local melt generation permits other pairs of $T_m$ and $L$. Given a rough constraint on the lithospheric structure ($L \approx$100–200 km), no $d$ = 1 mm grain size case is capable of satisfying both the tidal and melt-generation constraints (the mantle is too cold). With a $d$ = 1 cm grain size and $L$ = 100–200 km, we estimate that $T_m$ = 1625 ± 75 K.

**Table 3.** Sensitivity of Results to Bulk Structure Assumed[a]

| $\rho_c$ | 6700 | 7000 | 7300 | 7600 | kg m$^{-3}$ |
|---|---|---|---|---|---|
| $\rho_m$ | 3513 | 3526 | 3536 | 3544 | kg m$^{-3}$ |
| $R_c$ | 1766 | 1700 | 1643 | 1593 | km |
| $\rho_0$ | 3311 | 3300 | 3290 | 3281 | kg m$^{-3}$ |
| $k_2$ | 0.153 | 0.141 | 0.131 | 0.123 | - |
| $Q$ | 90 | 92 | 93 | 95 | - |

[a]The different combinations of mean mantle and core density ($\rho_m$ and $\rho_c$) and core radius $R_c$ all yield the observed bulk density and moment of inertia, assuming a 50 km thick crust with a density of 2900 kg m$^{-3}$. These different structures yield different $k_2$ Love numbers, evaluated at Phobos' synodic frequency. However, for a given set of thermal parameters (here we take $L$ = 150 km, $T_m$ = 1600 K, and $d$ = 1 cm), $Q$ scarcely changes.

## 5. Discussion

### 5.1. Robustness

[60] Our model involved both simplifications and the choice of poorly known parameter values. It is therefore important to explore the extent to which these factors are likely to affect our results.

[61] One important uncertainty is in the bulk structure of Mars adopted. In Table 3 we list a range of different structures, all of which satisfy the moment of inertia and bulk density constraints, but with different core radii and core and mantle mean densities. Calculations of pressure, rigidity, etc. are carried out exactly as in section 3, with similar thermal parameters as our nominal model ($T_m$ = 1600 K, $L$ = 150 km, and $d$ = 1 cm). As expected, the Love number shows systematic changes as the bulk density structure is changed. However, of much more interest is the fact that $Q$ is almost unchanged. This is because $Q$ is mainly controlled by what is happening immediately beneath the lithosphere (Figure 1d), and thus the bulk structure adopted does not greatly affect it. This result is important, because it means that uncertainties in the bulk structure of Mars will not greatly affect our conclusions. In other words, $Q$ depends a lot on $T_m$ and $d$ but rather little on the rigidity and density structure (which are the primary controls on $k_2$). Thus, to determine the temperature structure of Mars, $Q$ is the most important factor to model.

[62] Although our results are insensitive to the bulk structure, they are sensitive to factors which affect temperature, such as thermal expansivity. For instance, increasing $\alpha$ of olivine by 50% causes a change in the near-surface temperature structure (equation (6)) and results in a 10% reduction in $Q$.

[63] As discussed above, the fact that tidal $Q$ is lowest just beneath the lid means that our simplified treatment of phase changes at depth is unlikely to affect our conclusions. However, relaxing the assumption of anhydrous, melt-free conditions may have more significant consequences. The main effect of both melt and water is to significantly reduce the effective viscosity and thus to enhance dissipation. The mantle of Mars can still apparently generate melt, but the sparse and localized nature of recent volcanic activity makes it somewhat unlikely that the global $Q$ value will be significantly affected.

[64] The role of water is less clear. As reviewed in *Grott et al.* [2013], the present-day concentration of water in the Martian mantle is very uncertain. Water, if present, will depress the solidus [*Pommier et al.*, 2012] and alter the viscosity, thus potentially changing the thermal evolution and present-day lid thickness and temperature [e.g., *Hauck and Phillips*, 2002; *Morschhauser et al.*, 2011; *Ogawa and Yanagisawa*, 2012]. Although it seems likely that the presence of water will tend to enhance dissipation and lower $Q$ [e.g., *Karato and Jung*, 1998], a quantitative understanding of this effect is currently lacking. Likewise, there is currently little understanding of how iron content affects dissipation, although it seems to have a significant effect on viscosity [*Zhao et al.*, 2009]. Better experimental constraints on the effect on $Q$ of water and iron content would be valuable.

[65] In short, our anhydrous, melt-free case almost certainly represents a low-dissipation end-member case: almost any additional factor (water, melt, crustal pore fluids, turbulence in the fluid core) will probably increase dissipation and decrease $Q$. Our mantle temperature estimate of $1625 \pm 75$ K may therefore be regarded as an upper limit. For instance, a wet Martian mantle might be colder than this, yet still satisfy the tidal and melt-generation constraints.

[66] Although we have generally assumed $Q = 88 \pm 16$ based on the *Lainey et al.* [2007] results, the *Bills et al.* [2005] analysis yields a higher $Q$ ($170 \pm 20$; section 2). Inspection of Figures 2 and 3 shows that matching such a $Q$ would require mantle temperatures roughly 200 K colder than the values we have derived above. This again demonstrates that our estimate of $T_m$ represents an upper bound.

### 5.2. Implications

[67] We have argued above that the tidal $Q$ of Mars implies a present-day mantle potential temperature of $1625 \pm 75$ K for a grain size of 1 cm. This potential temperature is almost identical to the estimate by *Herzberg et al.* [2007] of $1613 \pm 60$ K for the Earth's upper mantle. Strikingly, two recent petrological analyses, based respectively on Fe, Si, and Th concentrations [*Baratoux et al.*, 2011] and pyroxene concentrations [*Baratoux et al.*, 2013], have reached exactly the same conclusion. Furthermore, these latter studies imply source depths for recent volcanism of $\approx$150 km, consistent with our estimates of $L$ discussed above. There are thus two independent lines of evidence supporting an Earth-like mantle potential temperature.

[68] On Earth, mantle grain size is affected by two competing effects [*Karato*, 1988]. Passage through the spinel-perovskite phase transition results in recrystallization and reduction in grain size, while grain growth is a continuous process with a rate which strongly increases as temperature increases. As a result, the equilibrium grain size is expected to depend on the frequency with which grains are cycled through the phase transition and the temperatures they experience. On Mars, grain growth will proceed as on Earth, but the (likely) absence of a spinel-perovskite phase transition means that this grain size reduction mechanism is unlikely to occur [*Demouchy et al.*, 2011]. Because Martian and terrestrial mantle temperatures appear to be so similar, one would therefore expect mantle grain sizes to be larger on Mars than on Earth. The grain size of the Earth's upper mantle is probably a few millimeters [e.g., *Karato*, 1984], less than our inferred Mars value and thus in line with expectations.

[69] Depending on the creep regime, a higher grain size for Mars could also imply a more viscous mantle. Assuming dry olivine in the diffusion creep regime [*Hirth and Kohlstedt*, 1995], a 1 cm grain size with $T = 1600$ K implies a viscosity of $2.8 \times 10^{21}$ Pa s. This is larger than estimates of the Earth's uppermost mantle viscosity which, based on postglacial rebound studies, range from a few times $10^{19}$ Pa s to a few times $10^{20}$ Pa s [*Cathles*, 1975].

[70] On the other hand, many Mars convection models implicitly or explicitly require substantially higher present-day mantle temperatures and lower mantle viscosities. For instance, the purely thermal model T7HCM in *Ogawa and Yanagisawa* [2011] has a present-day temperature of about 1800 K, implying a viscosity of about $10^{19}$ Pa s. Similarly, the parameterized evolution models EPT21 and STL21 of *Breuer and Spohn* [2003] have temperatures in the range 1900–1950 K, implying viscosities of about $2–3 \times 10^{19}$ Pa s. *Kiefer* [2003] assumed a core-mantle boundary temperature equivalent to a mantle potential temperature of 1804 K, somewhat above our inferred range. These low viscosities and high temperatures arise in thermal evolution models because stagnant lid convection is relatively inefficient at getting rid of heat, and thus the rate of cooling within Mars has been quite modest. In contrast, the lower temperatures in our models might have arisen from early rapid cooling of the Martian mantle, perhaps due to plate-tectonic-like behavior [*Nimmo and Stevenson*, 2000] or advection of melt. It will obviously be of future interest to reconcile these different approaches to estimating Martian interior properties.

[71] Studies of the interior of Mars are likely to undergo profound advances once the results from the *InSight* seismometer [*Lognonne et al.*, 2012] arrive. If Mars possesses a high-velocity lid (Figure 1c), that is a potentially detectable feature (for instance, if normal mode excitation occurs—see *Gudkova and Zharkov* [2004]). The seismic $Q$ structure of the Martian mantle (Figure 1d) may also be determined and must then be reconciled with the tidal $Q$. Other techniques may also prove valuable. In particular, the trade-off between mantle temperature and water content may ultimately be resolved by using electromagnetic sounding [*Civet and Tarits*, 2012].

## 6. Conclusions and Future Work

[72] The main conclusion of this paper is simple: the observed tidal $Q$ of Mars can be understood using laboratory-derived material parameters. An anhydrous, melt-free Martian mantle with a potential temperature similar to (but a grain size somewhat larger than) that of the Earth's upper mantle and a moderate-thickness lithosphere is consistent with the available tidal and melt-generation constraints. A wetter mantle might permit lower mantle potential temperatures without violating the tidal or melt-generation constraints.

[73] One obvious shortcoming in our approach is that dissipation models based on $Fo_{90}$ olivine may not be appropriate to the Martian mantle. It will therefore be of interest to carry out experimental studies into how iron content affects dissipation. Likewise, as noted above, this study and petrological studies have deduced lower mantle potential temperatures than some thermal evolution models. An obvious next step would be to take the output from some of

these evolution models and see whether their predicted tidal parameters are consistent with those observed. Ultimately, it is to be hoped that the *InSight* mission will lay many of the remaining discrepancies to rest.

[74] **Acknowledgments.** We thank Amir Khan for helpful discussion and Michael Efroimsky and an anonymous reviewer for comments which improved the manuscript.

## References

Baratoux, D., M. J. Toplis, M. Monnereau, and O. Gasnault (2011), Thermal history of Mars inferred from orbital geochemistry of volcanic provinces, *Nature*, *472*, 338–340.

Baratoux, D., M. J. Toplis, M. Monnereau, and V. Sautter (2013), The petrological expression of early Mars volcanism, *J. Geophys. Res. Planets*, *118*, 1–160, doi:10.1029/2012JE004234.

Bass, J. D. (1995), Elasticity of minerals, glasses and melts, in *Mineral Physics and Crystallography: A Handbook of Physical Constants*, edited by T. J. Ahrens, pp. 45–63, AGU, Washington, D. C.

Bertka, C. M., and Y. W. Fei (1997), Mineralogy of the Martian interior up to core-mantle boundary pressures, *J. Geophys. Res.*, *102*, 5251–5264.

Bertka, C. M., and Y. W. Fei (1998), Density profile of an SNC model Martian interior and the moment-of-inertia factor of Mars, *Earth Planet. Sci. Lett.*, *157*, 79–88.

Bertka, C. M., and J. R. Holloway (1994), Anhydrous partial melting of an iron-rich mantle. 1. Subsolidus phase assemblages and partial melting phase relations at 10 to 30 kbar, *Contrib. Min. Pet.*, *115*, 313–322.

Bills, B. G., G. A. Neumann, D. E. Smith, and M. T. Zuber (2005), Improved estimate of tidal dissipation within Mars from MOLA observations of the shadow of Phobos, *J. Geophys. Res.*, *110*, E07004, doi:10.1029/2004JE002376.

Breuer, D., and T. Spohn (2003), Early plate tectonics versus single-plate tectonics on Mars: Evidence from magnetic field history and crust evolution, *J. Geophys. Res.*, *108*, 5072, doi:10.1029/2002JE001999.

Castillo-Rogez, J. C., and B. W. Banerdt (2013), Impact of anelasticity on Mars' dissipative properties—Application to the Insight mission, paper presented at 44th Lunar and Planetary Science Conference, The Woodlands, Texas.

Cathles, L. M. (1975), *The Viscosity of the Earth's Mantle*, Princeton Univ. Press, Princeton, N. J.

Civet, F., and P. Tarits (2012), Mars internal structure derived from MGS magnetic data, paper presented at The Mantle of Mars: Insights from Theory, Geophysics, High-Pressure Studies and Meteorites, Houston, Texas.

Demouchy, S., D. Mainprice, A. Tommasi, H. Couvy, F. Barou, D. J. Frost, and P. Cordier (2011), Forsterite to wadsleyite phase transformation under shear stress and consequences for the Earth's mantle transition zone, *Phys. Earth Planet. Inter.*, *184*, 91–104.

Dohmen, R., and R. Milke (2010), Diffusion in polycrystalline materials: Grain boundaries, mathematical models, and experimental data, *Rev. Mineral. Geochem.*, *72*, 921–970.

Dreibus, G., and H. Wanke (1985), Mars: A volatile rich planet, *Meteoritics*, *20*, 367–382.

Efroimsky, M. (2012), Tidal dissipation compared to seismic dissipation: In small bodies, Earths and super-Earths, *Astrophys. J.*, *746*, 150, doi:10.1088/0004-637X/746/2/150.

Frost, H. J., and M. F. Ashby (1982), *Deformation Mechanism Maps: The Plasticity and Creep of Metals and Ceramics*, Pergamon Press, Oxford.

Gribb, T. T., and R. F. Cooper (1998), Low-frequency shear attenuation in polycrystalline olivine: Grain boundary diffusion and the physical significance of the Andrade model for viscoelastic rheology, *J. Geophys. Res.*, *103*, 27,267–27,279.

Grott, M., and D. Breuer (2010), On the spatial variability of the Martian elastic lithosphere thickness: Evidence for mantle plumes?, *J. Geophys. Res.*, *115*, E03005, doi:10.1029/2009JE003456.

Grott, M., et al. (2013), Long-term evolution of the Martian crust-mantle system, *Space Sci. Rev.*, *174*, 49–111.

Gudkova, T. V., and V. N. Zharkov (2004), Mars: Interior structure and excitation of free oscillations, *Phys. Earth Planet. Inter.*, *142*, 1–22.

Hartmann, W. K., M. Malin, A. McEwen, M. Carr, L. Soderblom, P. Thomas, E. Danielson, P. James, and J. Veverka (1999), Evidence for recent volcanism on Mars from crater counts, *Nature*, *397*, 586–589.

Hauck, S. A., and R. J. Phillips (2002), Thermal and crustal evolution of Mars, *J. Geophys. Res.*, *107*, 5052, doi:10.1029/2001JE001801.

Herzberg, C., P. D. Asimow, N. Arndt, Y. L. Niu, C. M. Lesher, J. G. Fitton, M. J. Cheadle, and A. D. Saunders (2007), Temperatures in ambient mantle and plumes: Constraints from basalts, picrites and komatiites, *Geochem. Geophys. Geosyst.*, *8*, Q02006, doi:10.1029/2006GC001390.

Hirschmann, M. M. (2000), Mantle solidus: Experimental constraints and the effects of peridotite composition, *Geochem. Geophys. Geosys.*, *1*, 1042, doi:10.1029/200GC000070.

Hirth, G., and D. Kohlstedt (1995), Experimental constraints on the dynamics of the partially molten upper-mantle- deformation in the diffusion creep regime, *J. Geophys. Res.*, *100*, 1981–2001.

Hirth, G., and D. Kohlstedt (2003), Rheology of the upper mantle and the mantle wedge: A view from the experimentalists, *AGU Geophys. Monogr.*, *138*, 83–105.

Jackson, I., and U. H. Faul (2010), Grainsize-sensitive viscoelastic relaxation in olivine: Towards a robust laboratory-based model for seismological applications, *Phys. Earth Planet. Inter.*, *183*, 151–164.

Jackson, I., U. Faul, J. FitzGerald, and B. Tan (2004), Shear wave attenuation and dispersion in melt-bearing olivine polycrystals 1. Specimen fabrication and mechanical testing, *J. Geophys. Res.*, *109*, B06201, doi:10.1029/2003JB002406.

Karato, S. (1984), Grain-size distribution and rheology of the upper mantle, *Tectonophysics*, *104*, 155–176.

Karato, S. (1988), The role of recrystallization in the preferred orientation of olivine, *Phys. Earth Planet. Inter.*, *51*, 107–122.

Karato, S., and H. Jung (1998), Water, partial melting and the origin of the seismic low velocity and high attenuation zone in the upper mantle, *Earth Planet. Sci. Lett.*, *157*, 193–207.

Kawazoe, T., S. Karato, J. Ando, Z. C. Jing, K. Otsuka, and J. W. Hustoft (2010), Shear deformation of polycrystalline wadsleyite up to 2100 K at 14–17 GPa using a rotational Drickamer apparatus (RDA), *J. Geophys. Res.*, *115*, B08208, doi:10.1029/2009JB007096.

Khan, A., and J. Connolly (2008), Constraining the composition and thermal state of Mars from inversion of geophysical data, *J. Geophys. Res.*, *113*, E07003, doi:10.1029/2007JE002996.

Kiefer, W. S. (2003), Melting in the Martian mantle: Shergottite formation and implications for present-day mantle convection on Mars, *Meteorit. Planet. Sci.*, *38*, 1815–1832.

Kiefer, W. S., and Q. Li (2009), Mantle convection controls the observed lateral variations in lithospheric thickness on present-day Mars, *Geophys. Res. Lett.*, *36*, L18203, doi:10.1029/2009GL039827.

Lainey, V., V. Dehant, and M. Paetzold (2007), First numerical ephemerides of the Martian moons, *465*, *E120031*, doi:10.1051/0004-6361:20065466.

Lognonne, P., and C. Johnson (2007), Planetary seismology, *Treatise Geophys.*, *10*, 69–116.

Lognonne, P., and B. Mosser (1993), Planetary seismology, *Surv. Geophys.*, *14*, 239–302.

Lognonne, P., et al. (2012), Insight and single-station broadband seismology: From signal and noise to interior structure determination, paper presented at 43rd Lunar and Planetary Science Conference, The Woodlands, Texas.

Longhi, J., E. Knittle, J. R. Holloway, and H. Wanke (1992), The bulk composition, mineralogy and internal structure of Mars, in *Mars*, edited by H. H. Kieffer et al., pp. 184–208, Univ. of Arizona Press, Tucson, Ariz.

Matas, J., and M. S. T. Bukowinski (2007), On the anelastic contribution to the temperature dependence of lower mantle seismic velocities, *Earth Planet. Sci. Lett.*, *259*, 51–65.

McGovern, P. J., S. C. Solomon, D. E. Smith, M. T. Zuber, M. Simons, M. A. Wieczorek, R. J. Phillips, G. A. Neumann, O. Aharonson, and J. W. Head (2004), Localized gravity/topography admittance and correlation spectra on Mars: Implications for regional and global evolution, *J. Geophys. Res.*, *109*, E07007, doi:10.1029/2004JE002286.

Mocquet, A., and M. Menvielle (2000), Complementarity of seismological and electromagnetic sounding methods for constraining the structure of the Martian mantle, *Planet Space Sci.*, *48*, 1249–1260.

Morschhauser, A., M. Grott, and D. Breuer (2011), Crustal recycling, mantle dehydration and the thermal evolution of Mars, *Icarus*, *212*, 541–558.

Nimmo, F., U. H. Faul, and E. J. Garnero (2012), Dissipation at tidal and seismic frequencies in a melt-free Moon, *J. Geophys. Res.*, *117*, E09005, doi:10.1029/2012JE004160.

Nimmo, F., and D. Stevenson (2000), The influence of plate tectonics on the thermal evolution and magnetic field of Mars, *J. Geophys. Res.*, *105*, 11,969–11,980.

Nishihara, Y., D. Tinker, T. Kawazoe, Y. S. Xu, Z. C. Jing, K. N. Matsukage, and S. I. Karato (2008), Plastic deformation of wadsleyite and olivine at high-pressure and high-temperature using a rotational Drickamer apparatus (RDA), *Phys. Earth Planet. Inter.*, *170*, 159–169.

Ogawa, M., and T. Yanagisawa (2011), Numerical models of Martian mantle evolution induced by magmatism and solid-state convection beneath stagnant lithosphere, *J. Geophys. Res.*, *116*, E08008, doi:10.1029/2010JE003777.

Ogawa, M., and T. Yanagisawa (2012), Two-dimensional numerical studies on the effects of water on Martian mantle evolution induced by magmatism and solid-state mantle convection, *J. Geophys. Res.*, *117*, E06004, doi:10.1029/2012JE004054.

Phillips, R., et al. (2008), Mars north polar deposits: Stratigraphy, age and geodynamical response, *Science*, *320*, 1182–1185.

Pommier, A., T. L. Grove, and B. Charlier (2012), Water storage and early hydrous melting of the Martian mantle, *Earth Planet. Sci. Lett.*, *333*, 272–281.

Ray, R. D., R. J. Eanes, and F. G. Lemoine (2001), Constraints on energy dissipation in the Earth's body tide from satellite tracking and altimetry, *Geophys. J. Int.*, *144*, 471–480.

Rivoldini, A., T. V. Hoolst, O. Verhoeven, and A. Mocquet (2011), Geodesy constraints on the interior structure and composition of Mars, *Icarus*, *213*, 451–472.

Roberts, J. H., and F. Nimmo (2008), Tidal heating and the long-term stability of a subsurface ocean on Enceladus, *Icarus*, *194*, 675–689.

Sohl, F., and T. Spohn (1997), The interior structure of Mars: Implications from SNC meteorites, *J. Geophys. Res.*, *102*, 1613–1635.

Sohl, F., G. Schubert, and T. Spohn (2005), Geophysical constraints on the composition and structure of the Martian interior, *J. Geophys. Res.*, *110*, E12008, doi:10.1029/2005JE002520.

Solomatov, V. S., and L. N. Moresi (1996), Stagnant lid convection on Venus, *J. Geophys. Res.*, *101*, 4737–4753.

Stixrude, L., and C. Lithgow-Bertelloni (2005), Thermodynamics of mantle minerals. I. Physical properties, *Geophys. J. Int.*, *162*, 610–632.

Stixrude, L., and C. Lithgow-Bertelloni (2011), Thermodynamics of mantle minerals. II. Phase equilibria, *Geophys. J. Int.*, *184*, 1180–1213.

Van Hoolst, T., V. Dehant, F. Roosbeek, and P. Lognonne (2003), Tidally induced surface displacements, external potential variations and gravity variations on Mars, *Icarus*, *161*, 281–296.

Vaucher, J., D. Baratoux, N. Mangold, P. Pinet, K. Kurita, and M. Gregoire (2009), The volcanic history of central Elysium Planitia: Implications for Martian magmatism, *Icarus*, *204*, 418–442.

Verhoeven, O., et al. (2005), Interior structure of terrestrial planets: Modelling Mars' mantle and its electromagnetic, geodetic and seismic properties, *J. Geophys. Res.*, *110*, E04009, doi:10.1029/2004JE002271.

Yoder, C. F., A. S. Konopliv, D. N. Yuan, E. M. Standish, and W. M. Folkner (2003), Fluid core size of Mars from detection of the solar tide, *Science*, *300*, 299–303.

Zhao, Y.-H., M. E. Zimmerman, and D. L. Kohlstedt (2009), Effect of iron content on the creep behavior of olivine: 1. Anhydrous conditions, *Earth Planet. Sci. Lett.*, *287*, 229–240.

Zharkov, V. N., and T. V. Gudkova (1997), On the dissipative factor of the Martian interiors, *Planet. Space Sci.*, *45*, 401–407.